INTERNATIONAL JOURNAL FOR NUMERICAL METHODS IN FLUIDS, VOL. 22, 467–481 (1996)

NUMERICAL CALCULATION OF 2D, UNSTEADY FLOW IN CENTRIFUGAL PUMPS: IMPELLER AND VOLUTE INTERACTION

D. CROBA AND J. L. KUENY

Centre de Recherche et d'Essais de Machines Hydrauliques de Grenoble, Institut National Polytechnique de Grenoble, BP 95, F-38402 St. Martin d'Hères, France

SUMMARY

A numerical model is developed for calculating the two-dimensional, unsteady, incompressible and turbulent flow within the rotating impeller and stationary volute of an industrial centrifugal pump. The objective is the investigation and comprehension of the instantaneous behaviour of centrifugal pumps, aiming at the reduction of vibrations, radial forces and hydraulic noise. The computation is performed within a blade-to-blade streamtube for the impeller and a tube normal to the axis of rotation for the volute. The equations to be solved are the unsteady Reynolds-averaged Navier–Stokes equations along with the continuity equation and the unsteady κ–ε equations for turbulence modelling. The finite volume method is applied for space discretization and an implicit scheme for time discretization. A multidomain overlapping grid technique is used for matching together the relative flow field calculated within the rotating impeller and the absolute one calculated within the stationary volute. In this way the impeller and volute interaction is directly taken into account. The numerical model is validated for a centrifugal pump of $N_q = 32$ under design flow conditions. Comparisons between calculation and measurements show fairly good agreement.

KEY WORDS: centrifugal pump; multidomain calculation; unsteady flow; finite volume method

1. INTRODUCTION

Flow in turbomachinery is turbulent, three-dimensional, unsteady, either compressible or incompressible, sometimes with two-phase and cavitation phenomena appearing. In addition to that, turbomachinery configurations are of great complexity, with several different parts, rotating and stationary ones. In spite of the astonishing evolution of computers and numerical methods, some simplifying assumptions have to be made for calculating turbomachinery flows. These assumptions have to be chosen carefully, taking into account the particular test case and the physical phenomena appearing. A numerical model for turbomachinery flow computation may be used as a tool (a) for design optimization, (b) for prediction of hydrodynamic performances and (c) for comprehension of the physical mechanisms involved.

According to the literature, unsteady flow in centrifugal pumps is responsible for vibrations, an important part of hydraulic noise,[1,2] fluctuating radial forces acting on the impeller as well as eccentric oscillations of it.[3] The unsteadiness of the flow is due to the rotation of the impeller (transportation in space), which is seen from the point of view of the stationary volute as a transportation in time. The unsteady wakes travelling downstream of the impeller blades impinge on the volute tongue, resulting in hydrodynamic fluctuations in both the impeller and volute. The volute tongue acts as an obstacle to the incoming unsteady flow and tends to amplify these fluctuations. Thus the instantaneous response of a centrifugal pump is a result of the impeller and volute interaction. The main difficulty in modelling

CCC 0271–2091/96/010467-15

Received June 1994
Revised April 1995

this interaction lies in the geometrical complexity of the two parts and in the relative motion of one with respect to the other.

Chapin[4] solves numerically the compressible, inviscid and three-dimensional flow field within a stationary blade cascade (stator) using the finite volume method. He sets as inlet condition a rotating, non-uniform, total pressure profile representing qualitatively the outlet of the rotor preceding the stator of the machine.

Fatsis[5] presents a three-dimensional, inviscid, unsteady, indifferently compressible or incompressible flow computation within the rotating part of a turbomachine using the finite volume method. He sets as outlet condition a non-uniform static pressure profile coming from measurements performed in advance in the considered configuration. The apparent inconvenience of this method is the need for experimental data.

Hureau[6] presents a numerical calculation of the two-dimensional, potential, quasi-steady and incompressible flow field within the impeller and volute of a centrifugal pump using the singularity method.

Morfiadakis *et al.*[7] perform a two-dimensional, inviscid, fully unsteady and incompressible computation within an industrial centrifugal pump, matching together the impeller and volute. They apply the boundary element method, which is appropriate for treating complex geometries but rather inconvenient for three-dimensional and viscous flow computations.

Miner *et al.*[8] perform a two-dimensional, potential, incompressible and quasi-steady computation within a laboratory centrifugal pump using the finite element method. For each different impeller–volute orientation a different impeller–volute computational mesh is generated, which increases the total computational time and inhibits a fully unsteady computation.

Badie[9] presents a similar two-dimensional, potential, incompressible and fully unsteady computation by applying the finite element method, with a zone of interface between the impeller and volute. This zone dispenses with the need for generating a different impeller–volute mesh for each different impeller–volute orientation. Thus this computation is faster than the previous one, permitting a fully unsteady state approach.

Rai and Madavan[10] present a numerical model calculating the two-dimensional, unsteady, compressible and viscous flow field within an axial turbine rotor–stator configuration. They solve the unsteady thin layer Navier–Stokes equations using patched and overlaid grids for matching together different computational domains.

Most works on unsteady flow in rotor–stator configurations simplify either the computational domain (e.g. only the rotor or stator is taken into account) or the flow field (e.g. potential or quasi-steady flow computation). The present work attempts a more realistic though two-dimensional approach, considering the flow fully unsteady, incompressible and turbulent. In fact, the unsteadiness of the flow and the viscosity of the working fluid are of primary importance for reliable instantaneous flow field predictions and cannot be neglected.[11] The assumption of two-dimensional flow is expected to have a strong impact on the computational results, which is nevertheless attenuated by a quasi-three-dimensional approach.

The equations to be solved are (a) the continuity equation, (b) the unsteady Reynolds-averaged Navier–Stokes equations and (c) the unsteady κ–ε equations for turbulence closure modelling.

2. COMPUTATIONAL DOMAIN—DISCRETIZATION

Figures 1(a) and 1(b) show the configuration of a centrifugal, mixed flow pump of a specific speed $N_q = 32$, designed and tested by CETIM (Centre Technique d'Industries Mécaniques). Figure 1(a) presents the meridian plane and Figure 1(b) the plane normal to the axis of rotation of the pump. Two main parts are distinguished: the rotating part, which is the impeller consisting of N_b blades, and the

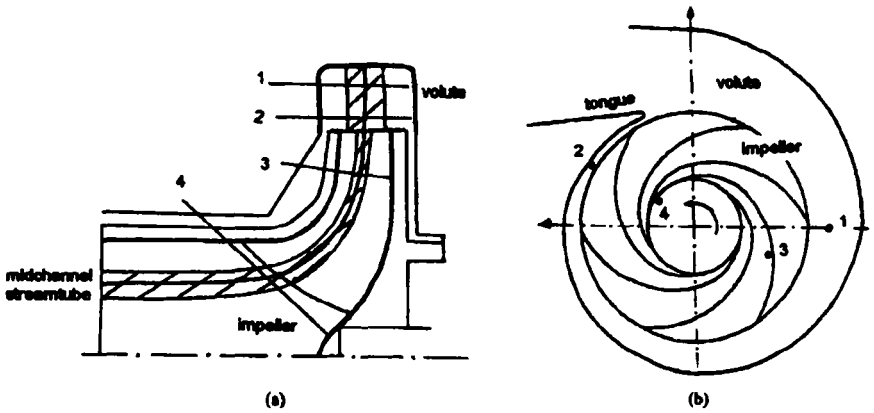

Figure 1. Centrifugal pump: (a) meridian plane; (b) plane normal to axis of rotation

stationary one, which is the volute. Note that the volute of the pump in question is two-dimensional, of rectangular cross-section.The volute tongue, often placed close to the impeller exit, is a featuring part of the volute.

2.1. *Impeller grid*

A blade-to-blade streamtube is considered placed at mid-section between the hub and tip at the impeller exit (streamtube $\Psi = 0{\cdot}5$; Figure 2). This blade-to-blade tube is obtained by an inviscid, steady state calculation performed in the meridian plane of the impeller.[12] Figure 3 shows the variation of the normalized flow field width throughout the impeller versus the meridian co-ordinate m for the mid-channel streamtube $\Psi = 0{\cdot}5$. This flow field width variation is incorporated into the blade-to-blade calculation performed within the impeller, through the spatial integration of the governing equations. In this way the two-dimensional computation resembles a quasi-three-dimensional one.

The computational domain is a single-blade flow passage with one blade placed at mid-section and two periodic lateral boundaries. For simplicity the blades are considered infinitesimally thin.

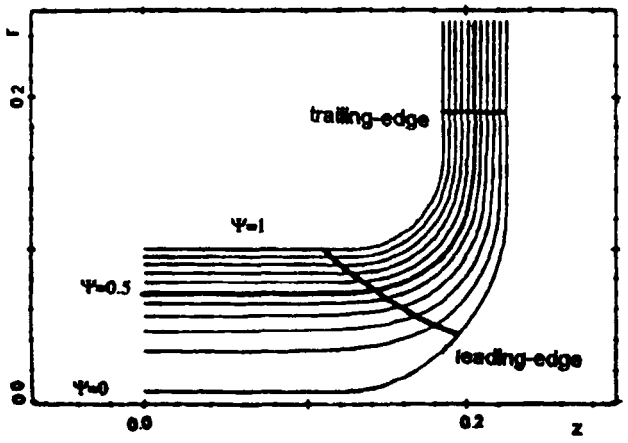

Figure 2. Impeller, meridian plane. Streamlines from $\Psi = 0$ to 1

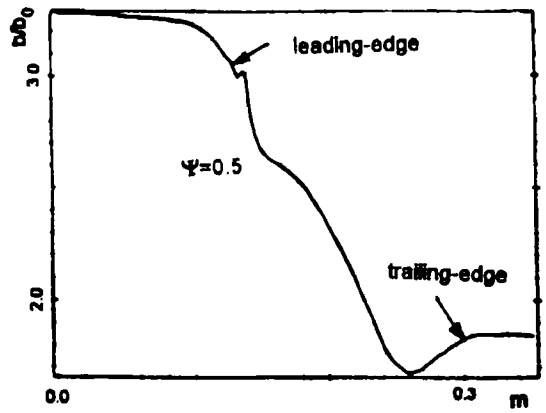

Figure 3. Normalized flow field width throughout impeller for $\Psi = 0{\cdot}5$

An orthogonal curvilinear grid of 'H' type is generated in a single-blade flow passage by solving the Laplace equations $\nabla^2\Phi = 0$ and $\nabla^2\Psi = 0$ of the potential and irrotational flow, applying the finite volume method.

2.2. *Volute grid*

The computational domain is a mid-section tube normal to the axis of rotation (Figures 1(a) and 1(b)). An orthogonal curvilinear grid is generated by solving the Laplace equations via the finite element method.

2.3. *Remarks on impeller and volute grid generation*

Figure 4 shows a zoom of the impeller and volute grids near the volute tongue. The impeller outlet and volute inlet circumference and not smooth lines but 'stepped' ones (Figures 5(a) and 5(b)). They

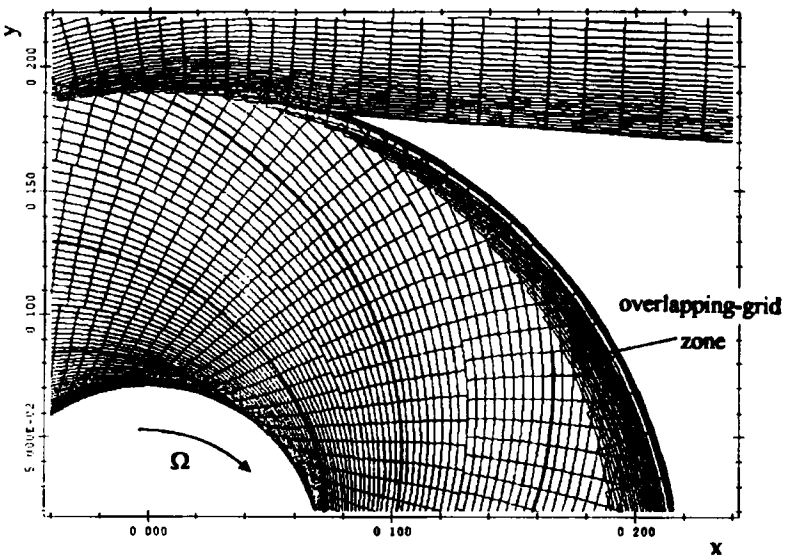

Figure 4. Impeller and volute grids. Zoom near the volute tongue

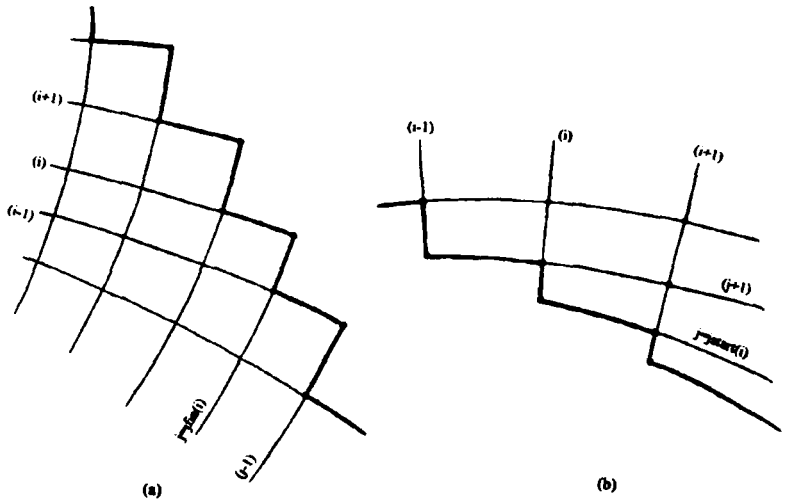

Figure 5. Grid 'cut into stairsteps': (a) impeller outlet; (b) volute inlet

will be referred to as boundaries 'cut into stairsteps'. Cutting a boundary into stairsteps is a special technique for treating computational domains of non-orthogonal boundaries with orthogonal curvilinear grids. The implementation of this technique does not present any particular difficulties and does not modify the general structure of a typical finite volume code. One only needs to solve the governing equations for $i=1$ to ni and $j=j(1)$ to $j(ni)$, where $j(i)=j(i-1)+1$, with $j(1)=1$ and $j(ni)=nj$, instead of solving them for $i=1$ to ni and $j=1$ to nj.

The impeller and volute grids are independently generated. Nevertheless, some restrictions are imposed on both grids, since they are meant to co-operate.

1. The outlet of the impeller grid should not overlap the volute solid wall. Attention has to be paid especially near the volute tongue, where the distance between the impeller outlet and the volute solid wall is often very small.
2. The inlet of the volute grid should not overlap the trailing edge of the blades.
3. A thin overlapping grid zone should be formed between the impeller and volute grids in order to match together the two domains by transmitting data from one to the other.
4. One would physically expect some abrupt gradients around the impeller outlet (volute inlet) circumference because of viscous wakes travelling downstream of the blades. Thus the impeller grid should be fine enough to enable good viscous wake simulation and the volute grid should be equally fine to enable good capture of the viscous wakes coming into the volute.

For the test case presented here (centrifugal pump of $N_q=32$), a 20×91 grid is generated within each single-blade flow passage of the impeller ($N_b=6$ flow passages in all) and a 132×152 grid within the volute.

3. GOVERNING EQUATIONS—DISCRETIZATION

The flow is considered two-dimensional, incompressible, viscous (turbulent) and unsteady. The working fluid is considered Newtonian. The governing equations in the impeller and volute are as follows:

continuity equation

$$\vec{\nabla}\vec{C} = 0 \tag{1}$$

unsteady Reynolds-averaged Navier–Stokes equations

$$\frac{\partial \vec{C}}{\partial t} + \vec{C}(\vec{\nabla}C_i) = -\frac{1}{\rho}\vec{\nabla}P + \vec{\nabla}[\Gamma_C(\vec{\nabla}C_i)] + \{\vec{F}_{\text{rot}}\}, \tag{2}$$

unsteady κ–ε equations for turbulence closure

$$\frac{\partial \kappa}{\partial t} + \vec{C}(\vec{\nabla}\kappa) = \vec{\nabla}[\Gamma_\kappa(\vec{\nabla}\kappa)] + \frac{G}{\rho} - \varepsilon, \tag{3}$$

$$\frac{\partial \varepsilon}{\partial t} + \vec{C}(\vec{\nabla}\varepsilon) = \vec{\nabla}[\Gamma_\varepsilon(\vec{\nabla}\varepsilon)] + \frac{\varepsilon}{\kappa}\left(C_1\frac{G}{\rho} - C_2\varepsilon\right), \tag{4}$$

where $\Gamma_C = \nu_{\text{eff}}$, $\Gamma_\kappa = \nu_{\text{eff}}/\sigma_\kappa$, $\Gamma_\varepsilon = \nu_{\text{eff}}/\sigma_\varepsilon$ and $\nu_{\text{eff}} = \nu + \nu_t$.

In the above equations $\vec{C}$ is the velocity vector, C_i $(i = 1,2)$ are the two velocity components, P is the static pressure, κ is the turbulent kinetic energy and ε its dissipation rate, G is the generation rate of turbulent kinetic energy, ρ is the density of the fluid and ν its kinematic viscosity, ν_t is the turbulent kinematic viscosity according to the Boussinesq theorem and σ_κ, σ_ε, C_1 and C_2 are empirical constants of the κ–ε model.

The above equations refer to both the impeller and volute. However, the symbol C stands for the absolute velocity in the volute where the computation takes place in the absolute (stationary) frame of reference, but for the relative velocity in the impeller where the computation takes place in the relative frame (rotating with an angular velocity Ω).

The force F_{rot} placed in brackets in the momentum equation (2) exists solely for the impeller calculation and is written as

$$\vec{F}_{\text{rot}} = \vec{F}_{\text{Coriolis}} + \vec{F}_{\text{centrifugal}}, \tag{5}$$

$$\vec{F}_{\text{Coriolis}} = 2(\vec{\Omega} \wedge \vec{W}), \qquad \vec{F}_{\text{centrifugal}} = \vec{\Omega} \wedge (\vec{\Omega} \wedge \vec{r}), \tag{6}$$

where $\vec{\Omega}$ is the angular velocity of rotation of the impeller, $\vec{r}$ is the radial co-ordinate and $\vec{W}$ is the relative velocity vector of the rotating impeller.

The turbulent kinematic viscosity ν_t is given by the formula $\nu_t = C_D\kappa^2/\varepsilon$, where C_D is an empirical constant of the κ–ε model.

Initially the standard κ–ε turbulence closure model[13] was applied for the impeller-volute modelling, as it is widely tested and has a well-known computational behaviour, though it is rather inadequate for rotating flows. An improved version of the κ–ε model, accounting for rotating computational domains, is to be incorporated in the code at a later stage.

All the above equations expressed in an orthogonal curvilinear system of co-ordiantes (ξ, η) may be written in the general form

$$\frac{\partial \Phi}{\partial t} + \frac{1}{h_1 h_2}\frac{\partial}{\partial \xi}(\Phi u h_2) + \frac{1}{h_1 h_2}\frac{\partial}{\partial \eta}(\Phi v h_1) = \frac{1}{h_1 h_2}\frac{\partial}{\partial \xi}\left(\Gamma_\Phi \frac{h_2}{h_1}\frac{\partial \Phi}{\partial \xi}\right) + \frac{1}{h_1 h_2}\frac{\partial}{\partial \eta}\left(\Gamma_\Phi \frac{h_1}{h_2}\frac{\partial \Phi}{\partial \eta}\right) + S_\Phi, \tag{7}$$

where Φ stands for 1, u, v, κ or ε indifferently, Γ_Φ is the diffusion coefficient, S_Φ is the source term, u and v are the velocity components along co-ordinates ξ and η respectively and h_1 and h_2 are the metric coefficients of the orthogonal co-ordinate system.

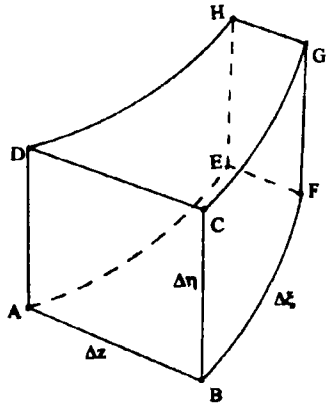

Figure 6. Bitrapezoidal element for integration of governing equations

The finite volume method is applied for the space discretization of equation (7) and the SIMPLE algorithm for staggered grids is utilized for linking the velocity and pressure fields.[14] For the discretization of the convection terms the hybrid upwind–central finite difference scheme is applied. The underrelaxation method is used for stabilizing the resulting system of equations during the iterative procedure. The optimum underrelaxation factors are found to be especially low, of the order of 0·01. The Gauss–Seidel routine is used for solving the algebraic system of equations.

An unconditionally stable first-order implicit scheme is applied for the time discretization. The time-dependent term is then expressed as

$$\frac{\partial \Phi}{\partial t} \approx \frac{\Phi^{t+\Delta t} - \Phi^t}{\Delta t}, \tag{8}$$

where Δt is the considered time step.

Equation (7) may then be written in the general form

$$(A_P - S_1)\Phi_P = A_N\Phi_N + A_S\Phi_S + A_E\Phi_E + A_W\Phi_W + S_2, \tag{9}$$

where S_1 and S_2 come from the linearization of the source term $S_\Phi = S_1\Phi_P + S_2$.

Note that the flow field is considered two-dimensional, since only two velocity components u and v are taken into consideration, but the grid cells for this computation are three-dimensional (bitrapezoidal elements; Figure 6). Thus, when equation (7) is integrated in space in order to be discretized, a volume element $\Delta V = \Delta\xi\Delta\eta\Delta z$ is considered and not a surface one $\Delta A = \Delta\xi\Delta\eta$. In this way the flow field width variation throughout the computational domain is taken into account, the two-dimensional calculation resembling a quasi-three-dimensional one.[5]

4. BOUNDARY AND INITIAL CONDITIONS—COMPUTATIONAL PROCEDURE

Boundary conditions are set at the inlet and the outlet of the pump (impeller inlet and volute outlet respectively), considering that the dynamic interaction of the pump and the piping system is negligible and the inlet and outlet of the computational domain are placed sufficiently far away from the impeller blades and volute tongue. The velocity is set at the impeller inlet, calculated through the flowrate Q and the rotational speed N of the pump. The pressure is set constant at the volute exit ($P = P_0$). At the solid

wall boundaries of the impeller and the volute the velocity is set to zero and wall-functions are applied for simulating the different boundary layer zones. Moreover, boundary conditions for k and ε are set at the impeller inlet ($k = 10^{-5}$ and $\varepsilon = 0$) and the volute outlet (Neumann condition: zero normal derivative). These boundary conditions would suffice for the computation of the flow within the centrifugal pump in case that it was considered as one computational domain. However, the fact that the pump consists of two components, one rotating and the other stationary, requires that those are treated as two separate computational domains, with a zone of interface between them for matching them together. In that case, boundary conditions are also needed at the zone of interface (impeller outlet and volute inlet), which are at the outset unknown. The following iterative procedure is then implemented.

Suppose that the pressure at the impeller outlet is known (an initial guess). Then, a computation can be performed within the impeller providing the velocity and pressure fields. The velocity field in the impeller being known, the velocity distribution around the volute inlet circumferance can be calculated through bilinear interpolations. Note that there is an overlapping-grid zone between the impeller and the volute, so that the volute inlet circumference is placed upstream of the impeller outlet circumference. The velocity distribution around the volute inlet circumference is set as volute inlet condition and then a computation can be performed within the volute, providing the velocity and pressure fields. The pressure field in the volute being known, the pressure distribution around the impeller outlet circumference can be calculated through bilinear interpolations. Now another computation can be performed within the impeller in order to update the impeller velocity field. *Once* the velocity field updated, another computation is performed within the volute to update the volute pressure field there, and so on, until convergence for the velocity and pressure fields is achieved within both domains.

Since this is an unsteady-state computation, the aforementioned procedure is carried out for each time instant t (for $t = \Delta t$, $t = 2\Delta t$, etc., where Δt is the time-step considered), until the fully periodical flow field is obtained, that is until the velocity and pressure fields in the volute repeat themselves for two successive blade passings of the impeller. As initial condition for this computation ($t = 0$) the steady-state flow field for the impeller and the volute is considered.

The impeller may be treated either as one computational domain with grid dimensions $N_b \times (ni \times nj)$, or as N_b separate subdomains (single-blade flow passages) with grid dimensions $ni \times nj$. The latter is preferable for this simulation in order to save computational time and memory. The flow field is calculated separately in each subdomain, information being transmitted from one subdomain to the other through the lateral boundaries (zones of interface). Suppose that $\Delta\theta = 2\pi/N_b$ is the blade-to-blade pitch of the impeller. Within a time-step Δt an impeller blade sweeps an angular interval $\delta\theta$, where: $\delta\theta = \Omega\Delta t$. The time-step Δt is determined so that there is an integer number N_{ts} of angular intervals $\delta\theta$ for the pitch $\Delta\theta$ to the swept by a blade: $\Delta\theta = N_{ts}\delta\theta = N_{ts}\Omega\Delta t$. An impeller blade, say N_p, and the corresponding subdomain, will be found at the time instant t at the position occupied by the following blade (subdomain) $N_p + 1$ at an earlier time instant $t - N_{ts}\Delta t$. The flow field calculated within the subdomain $N_p + 1$ at the time instant $t - N_{ts}\Delta t$ is stored and used as initial guess to start the computation in the subdomain N_p at the instant t. This technique is proved to accelerate the convergence for each time step and to reduce the total computation time (Fatsis[5]).

Periodicity is obtained with a precision of 10^{-2} after 15 to 18 impeller rotations, depending on the configuration and the flow conditions of the pump. The total CPU time required for such a computation is of the order of 80–100 hours on a HP-750 workstation. It is proved preferable to carry out a great number of subdomain-to-subdomain passings for each instant t, without caring for a strict convergence within each subdomain during each passing. In this way the coupling of different subdomains through boundary conditions is strengthened.

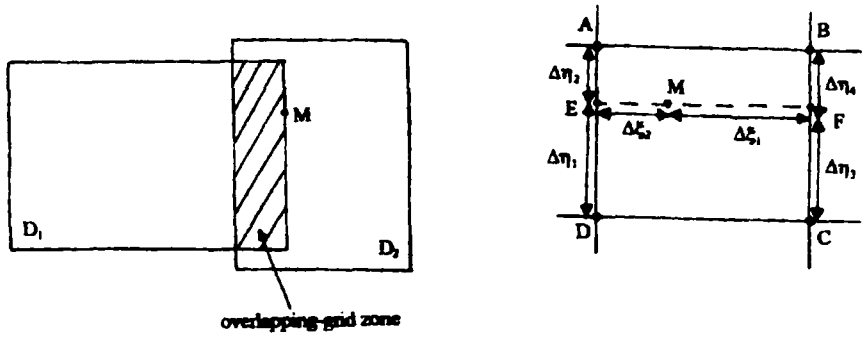

Figure 7. Bilinear interpolations. Node M at boundary of domain D_1

5. OVERLAPPING GRID TECHNIQUE

A multidomain overlapping grid technique[15,16] is applied to interpolate (a) the static pressure κ and ε distributions at the impeller outlet circumference, from the respective fields calculated within the volute, (b) the absolute velocity, κ and ε distributions at the volute inlet circumference, from the respective fields calculated within the impeller, and (c) the relative velocity static pressure κ and ε distributions on the lateral boundaries of a single-blade flow passage of the impeller, from the respective fields calculated within the adjacent single-blade flow passages.

Suppose that Φ is the unknown variable (standing for u, v, P, κ or ε indifferently) and M is a computational grid node at the boundary (inlet, outlet or lateral boundary indifferently) of the considered domain D_1. Suppose that D_2 is the adjacent domain where Φ is already calculated and known. The computational grids are generated so that there appears a thin overlapping grid zone between the domains D_1 and D_2. In this way the grid node M on the boundary of D_1, is surrounded by the grid nodes A–D of D_2 (Figure 7). The values of Φ at the above nodes will then be Φ_A, Φ_B, Φ_C and Φ_D respectively. The value Φ_M at M may then be calculated through bilinear interpolations as follows:

$$\Phi_E = F_1\Phi_A + (1 - F_1)\Phi_D, \qquad \Phi_F = F_2\Phi_B + (1 - F_2)\Phi_C, \qquad \Phi_M = F_3\Phi_E + (1 - F_3)\Phi_F,$$

where $F_1 = \Delta\eta_1/(\Delta\eta_1 + \Delta\eta_2)$, $F_2 = \Delta\eta_3/(\Delta\eta_3 + \Delta\eta_4)$ and $F_3 = \Delta\xi_1/(\Delta\xi + \Delta\xi_2)$ (Figure 7).

6. COMPUTATIONAL RESULTS

As test case for validating the numerical model, the flow within a centrifugal pump of a specific speed $N_q = 32$ is calculated (Figures 1(a) and 1(b)). A campaign of measurements has been conducted by CETIM (Croba, Kueny, Hureau and Kermarec[17]), focused on the instantaneous velocity field in the impeller and the volute of this pump, for design flow conditions. The objective of these measurements was the investigation of the instantaneous performances of the pump, and the comprehension of the sources of vibrations and hydraulic noise, at design flow conditions. The main characteristics of the $N_q = 32$ pump are shown in Table I. The unsteady, incompressible, two-dimensional (accounting for the flow field width variation) and turbulent flow is calculated within this pump for design flow conditions: $Q_n = 0{\cdot}136\ m^3/s$, $N_n = 1450$ rpm.

Figure 8 shows the instantaneous static pressure distribution around the volute inlet circumference for five different time instants: t, $t + 2\Delta t$, $t + 4\Delta t$, $t + 6\Delta t$ and $t + 8\Delta t$, that is for five different impeller orientations with respect to the volute tongue. The time-averaged static pressure distribution is

Table I. Characteristics of $N_q = 32$ centrifugal pump

$D_1 = 200$ mm diameter at impeller inlet
$D_2 = 380$ mm diameter at impeller outlet
$B_2 = 40$ mm width at impeller outlet
$D_3 = 392$ mm diameter at volute inlet
$B_3 = 80$ mm width at volute inlet
$H_{static} = 29{\cdot}9$ m static head of impeller
$P_{mech} = 61{\cdot}8$ kW mechanical power

also indicated by a thicker line. Note that the flow field in the volute is periodic for the instants t and $t + 10\Delta t$ ($N_{ts} = 10$ for this test case). Pressure is normalized by the factor $\Delta P = 0{\cdot}5\ \rho C_{in}^2$, where C_{in} is the radial velocity component at the pump inlet ($C_{in} = 4{\cdot}36$ m/s $\Rightarrow \Delta P = 9{\cdot}5$ kPa). An instantaneous pressure distortion appears around the volute inlet circumference, which is clearly stronger near the volute tongue. For the time instant $t + 4\Delta t$, when an impeller blade is found just opposite the volute tongue, the instantaneous pressure distortion attains its maximum value. The time-averaged pressure distortion around the volute inlet is about 9·5 kPa, while for this pump the impeller elevation is about 300 kPa. Note that this pressure distortion at the volute inlet is calculated assuming a uniform velocity profile at the impeller inlet and a uniform pressure profile at the volute outlet. The strong pressure pulsations at the volute inlet circumference illustrated in Figure 8 are, according to literature (Guelich and Bolleter[1]), responsible for the greatest part of hydraulic noise of centrifugal pumps.

Figures 9(a) and 9(b) show the instantaneous circumferential and radial absolute velocity distributions around the volute inlet circumference for three different impeller-volute orientations (time instants t, $t + 4\Delta t$, $t + 8\Delta t$). The thicker line indicates the time-averaged velocity profiles. Two terms are distinguished.

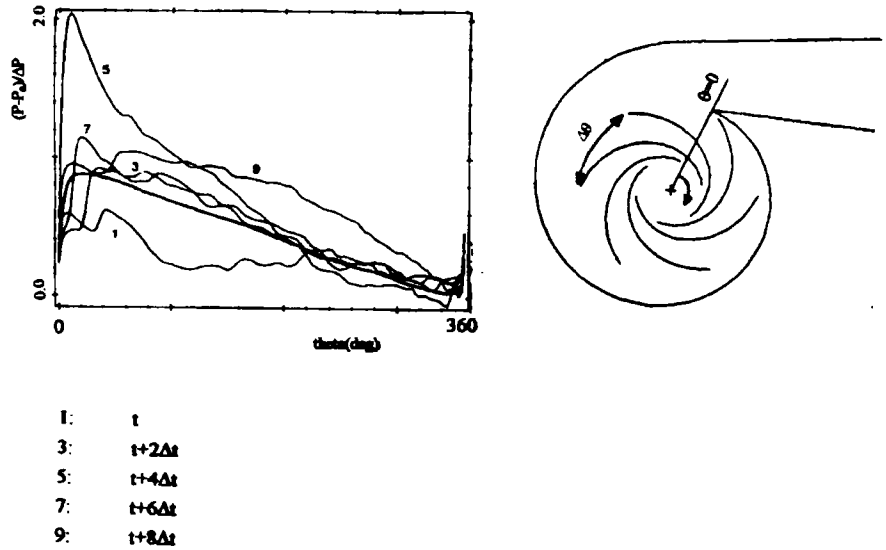

Figure 8. Instantaneous static pressure profile around volute inlet circumference: 1, t; 3, $t + 2\Delta t$; 5, $t + 4\Delta t$; 7, $t + 6\Delta t$; 9, $t + 8\Delta t$

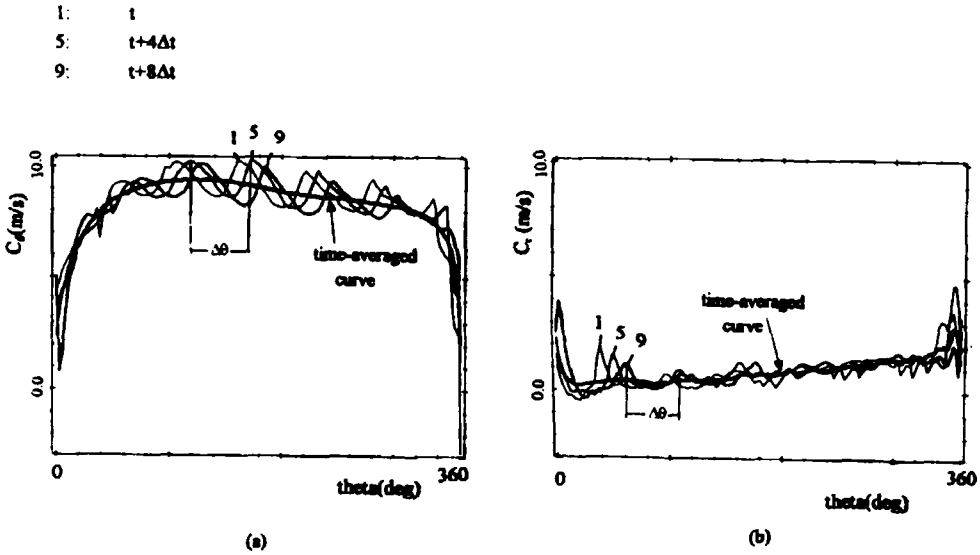

Figure 9. Instantaneous absolute velocity profile at volute inlet: (a) circumferential component; (b) radial component; 1, t; 5, $t+4\Delta t$; 9, $t+8\Delta t$

(a) A term due to the presence of the volute and, in particular, of the tongue, which is clearly distinguished on the time-averaged curves as circumferential velocity distortion maximized near the volute tongue.
(b) A term due to the blade passing, appearing on the instantaneous curves as peaks corresponding to the viscous wakes travelling downstream of the impeller blades.

These terms are also found in literature in the works of Yuasa and Hinata,[18] Sideris and van den Braembussche.[19] As seen in Figure 9(b), the radial velocity component attains instantaneously zero or even negative values in the vicinity of the volute tongue. This indicates that the incoming flow to the volute is instantaneously blocked up near the tongue, a fact that is qualitatively confirmed by measurements in other centrifugal pumps (Dong, Chu and Katz[20]).

A validation of the numerical model will now be attempted through comparisons with measurements of the instantaneous velocity within the impeller and the volute of the $N_q = 32$ pump for design flow conditions.

Figures 10 and 11 show that circumferential and radial absolute velocity components versus time, from t to $t + T$, (where $T = N_b N_{ts} \Delta t$ is the rotational period of the impeller) at points 1 and 2 of the volute respectively. Point 1 is placed far away from the volute tongue and the impeller outlet, while point 2 is close to both of them as seen in Figure 1(b). A very good agreement calculation-measurements is observed for point 1. The velocity profile is practically flat, which means that the viscous wakes travelling downstream of the blades are completely dissipated at point 1. For point 2, on the other hand, some strong velocity fluctuations appear, indicating that the viscous wakes are not dissipated yet. This happens because: (a) point 2 is close to the impeller outlet and (b) the proximity of the volute tongue tends to amplify the existent fluctuations. The above results agree qualitatively with literature (Miner, Beaudoin and Flack[21], Hamkins and Flack[22]). The amplitudes as well as the phases of the velocity fluctuations at point 2 are well predicted, except for the radial velocity component where the measured amplitude is under-estimated by the computation. In return, the calculated mean value is half as strong as the measured one for both velocity components, because of the abrupt widening of the flow field width when passing from the impeller outlet to the volute inlet (widths of 40 mm and 80 mm

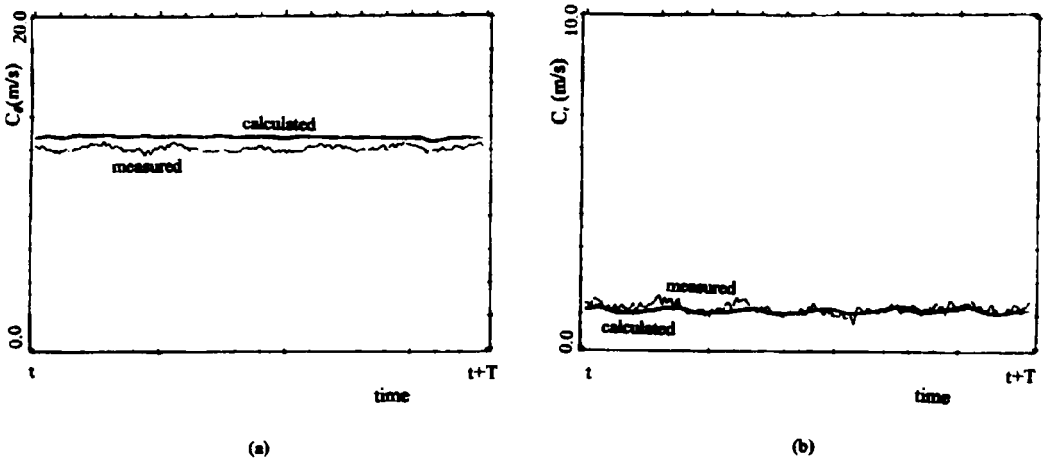

Figure 10. Point 1 (volute) instantaneous absolute velocity profile versus time: (a) circumferential component; (b) radial component

respectively). This abrupt widening is imposed by the particular impeller-volute design of the $N_q = 32$ pump (see Figure 1 and Table I). To respect the continuity of mass when passing from the impeller to the volute the radial velocity component is divided by a factor of 2 and to respect the continuity of streamline inclination at the same point the circumferential velocity component is divided by the same factor. This manipulation of the circumferential and radial components is contestable, since it modifies the angular momentum ($C_\theta r$) coming into the volute and it is susceptible of modifying the volute design flow conditions. This may explain the strong pressure distortion at the volute inlet (Figure 8). Note, however, that no such processing is required for a common centrifugal pump of conventional design, where the inlet volute width is equal to the impeller outlet width. Hence, this manipulation is applied only to the specific pump and it may by no means be considered as part of the numerical code presented here.

Figures 12 and 13 show the circumferential and radial absolute velocity components versus time (from t to $t + T$), at points 3 and 4 of the impeller respectively, as seen from the stationary frame of reference (Figure 1(b)). For point 3 there is a good agreement calculation-measurements regarding the

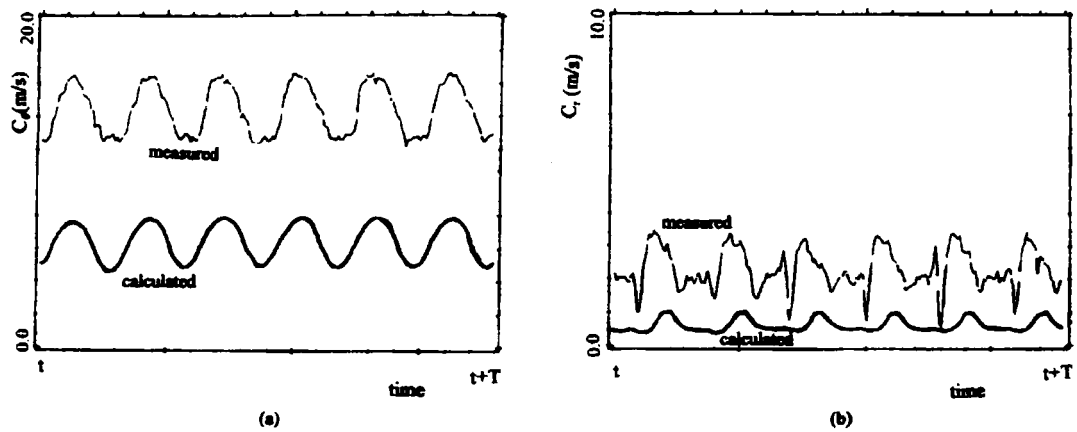

Figure 11. Point 2 (volute) instantaneous absolute velocity profile versus time: (a) circumferential component; (b) radial component

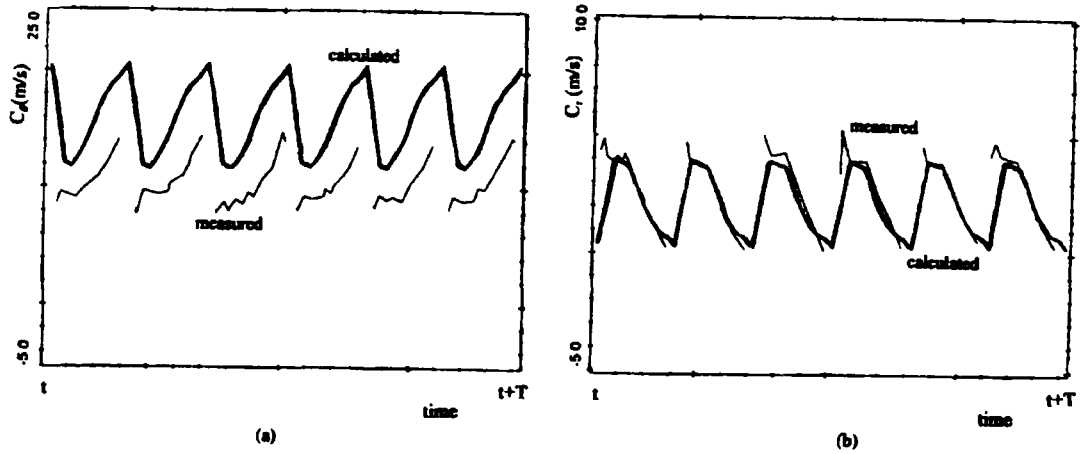

Figure 12. Point 3 (impeller) instantaneous absolute velocity profile versus time: (a) circumferential component; (b) radial component

radial velocity component, while the mean value and the amplitude of the circumferential velocity component seem to be overestimated by the computation. Note, however, that the profiles of measured velocity at point 3 are quite incomplete, because of the practical difficulties in conducting measurements within the rotating impeller. For point 4 the comparison calculation-measurements is less satisfactory, because: (a) The thickness of the blades is considered negligible for this computation, though it is certainly important near the leading-edge of the blades; (b) The streamtube considered for the computation (Figure 1(a)) and the one considered for the measurements are found not to coincide at the impeller inlet (difference in radius of about 10%). Velocity at computational point 4 and velocity at experimental point 4 are all the more not comparable as there is an important velocity gradient at the impeller inlet from hub to tip.

This numerical model is conceived for predicting the instantaneous performances of centrifugal pumps, but it may, all the more reason, be used for predicting overall performances. For instance, the measured static head of the impeller of the $N_q = 32$ pump is $H_{static} = 29{\cdot}9$ m. The calculated one is $H_{static} = (Pm_{outlet} - Pm_{inlet})/(\rho g) = 30{\cdot}7$ m, where Pm_{outlet} and Pm_{inlet} are the time-averaged pressures

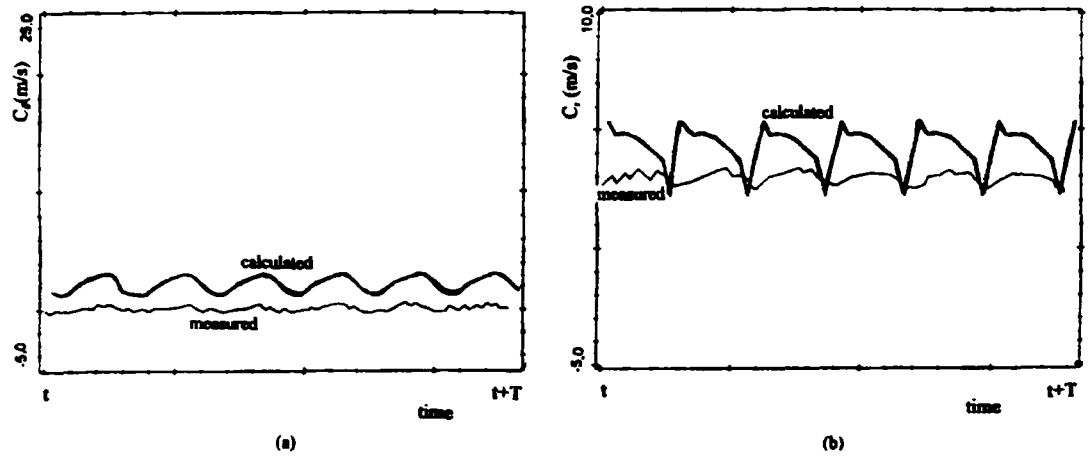

Figure 13. Point 4 (impeller) instantaneous absolute velocity profile versus time: (a) circumferential component; (b) radial component

at the impeller outlet and inlet respectively. There only appears a difference of 2·6% between calculation and measurements.

7. CONCLUSIONS

A numerical model has been developed for calculating the two-dimensional, unsteady, incompressible and turbulent flow simultaneously within the rotating impeller and stationary volute of industrial centrifugal pumps. The flow field width variation throughout the impeller has also been taken into account for this computation. The finite volume method was applied to discretize the governing equations in space and an implicit scheme to discretize them in time. A multidomain overlapping grid technique was used for matching together the different computational subdomains. As a test case the flow field within a centrifugal pump of $N_q = 32$ was calculated under design flow conditions. The physical aspect of the instantaneous performances of centrifugal pumps, as reported in literature, was accurately predicted by the model. Comparison between calculation and measurements regarding the instantaneous velocity field showed fairly good agreement, in particular far away from the volute tongue. Further improvements in the numerical model are to be undertaken, such as (a) application of a second-order numerical scheme for the convection terms (e.g. QUICK scheme), (b) application of an improved version of the κ–ε turbulence closure model, adequate for rotating flow fields, and (c) improved inlet and outlet conditions for the pump, taking into consideration the pump–piping system interaction. In reality there appear some pressure pulsations at the volute exit and some flow rate pulsations at the impeller inlet which may be of primary importance for the instantaneous response of the pump. (d) A quasi-three-dimensional computation is to be undertaken in the impeller and volute to improve the model performances near some difficult zones such as the volute tongue.

ACKNOWLEDGEMENTS

This work was supported by the French Army (DRET) and the CETIM (Centre Technique d'Industries Mécaniques).

APPENDIX: NOMENCLATURE

ξ, η	orthogonal curvilinear co-ordinates
x, y	Cartesian co-ordinates
i, j	serial numbers of grid lines along ξ- and η-directions
ni, nj	maxima of i and j
m, r, θ	meridian, radial and angular co-ordinates
Φ, Ψ	scalar potential and streamfunction
h_1, h_2	metric coefficients of orthogonal curvilinear co-ordinate system
F_1, F_2, F_3	coefficients of linear interpolations
u, v	velocity components along ξ- and η-directions
P	static pressure
κ	turbulent kinetic energy
ε	turbulent kinetic energy rate of dissipation
ρ	density of fluid
ν	kinematic viscosity of fluid
ν_t	turbulent kinematic viscosity
ν_{eff}	effective kinematic viscosity
$\sigma_\kappa, \sigma_\varepsilon, C_1, C_2, C_D,$	empirical constants of κ–ε model
Γ_Φ, S_Φ	diffusion coefficient and source term

$\vec{C}, \vec{W}$	absolute and relative velocity vectors
C_θ, C_r	circumferential and radial absolute velocity components
$\vec{\Omega}$	angular velocity vector of rotating impeller
$\vec{F}_{\text{Coriolist}}, \vec{F}_{\text{centrifugal}}$	Coriolis and centrifugal forces
$t, \Delta t$	time instant and time step
$Q\ (Q_n)$	flow rate (nominal)
$N\ (N_n)$	rotational speed (nominal)
N_q	specific speed
N_b	number of impeller blades
N_{ts}	total number of time steps for one blade to sweep a single-blade flow passage or a blade-to-blade pitch
$\Delta\theta$	blade-to-blade pitch
$\delta\theta$	angle swept by a blade in time interval Δt

REFERENCES

1. J. F. Guelich and U. Bolleter, 'Pressure pulsations in centrifugal pumps', *J. Vibr. Acoust.*, **114**, 272–279 (1992).
2. W. Neise, 'Review of noise reduction methods for centrifugal fans', *J. Eng. Ind.*, **104**, 151–161 (1982).
3. D. R. Adkins and C. E. Brennen, 'Analyses of hydrodynamic radial forces on centrifugal pump impellers', *J. Fluids Eng.*, **110**, 20–28 (1988).
4. V. Chapin, 'Contribution à la simulation numérique de l'interaction aérodynamique de deux roues ailetées', *Ph.D. Thesis*, Université Pierre et Marie Curie, Paris VI, 1993.
5. A. Fatsis, 'Three dimensional unsteady flow calculations in radial components', in *Lecture Series 1993–01, Spacecraft Propulsion*, von Karman Institute for Fluid Dynamics, Brussels, 1993.
6. F. Hureau, 'Méthode théorique et expérimentale de caractérisation des ecoulements instantionnaires dans les pompes centrifuges', *Ph.D. Thesis*, Université de Nantes, 1989.
7. E. E. Morfiadakis, S. G. Voutsinas and D. E. Papantonis, 'Unsteady flow calculation in a radial flow centrifugal pump with spiral casing', *Int. j. numer. methods fluids*, **12**, 895–908 (1991).
8. S. M. Miner, R. D. Flack and P. E. Allaire, 'Two-dimensional flow analysis of a laboratory centrifugal pump', *J. Turbomach.*, **114**, 333–339 (1992).
9. R. Badie, 'Analysis of unsteady potential flows in centrifugal pumps. Analytical and finite-element calculations in a centrifugal volute pump', *Ph.D. Thesis*, Mechanical Engineering Department, University of Twente, Enschede, 1993.
10. M. M. Rai and N. K. Madavan, 'Multi-airfoil Navier–Stokes simulations of turbine rotor–stator interaction', *J. Turbomach.*, **112**, 377–384 (1990).
11. D. Croba and J. L. Kueny, 'Unsteady flow computation in a centrifugal pump. Coupling of the impeller and the volute', *Proc. Int. INCE Symp. for Fan Noise*, Senlis, 1992, pp. 221–228.
12. T. Katsanis and W. D. McNally, 'Revised FORTRAN program for calculating velocities and streamlines on the hub-shroud midchannel stream surface of axial, radial or mixed flow turbomachines of annular duct', *NASA TN D-8431*, 1977.
13. B. E. Launder and D. B. Spalding, *Lectures in Mathematical Models of Turbulence*, Academic, New York, 1972.
14. S. V. Patankar and D. B. Spalding, 'A calculation procedure for heat, mass and momentum transfer in three-dimensional parabolic flows', *Int. J. Heat Mass Transfer*, **15**, 1787–1806 (1972).
15. M. C. Thompson and J. H. Ferziger, 'An adaptive multi-grid technique for the incompressible Navier–Stokes equations', *J. Comput. Phys.*, **82**, 94–121 (1989).
16. M. M. Rai, &'Navier–Stokes simulations of rotor–stator interaction using patched and overlaid grids', *AIAA J. Propuls. Power*, **3**, 387–396 (1987).
17. D. Croba, J. L. Kueny, F. Hureau and J. Kermarec, 'Numerical and experimental unsteady flow analysis in centrifugal pumps. Impeller and volute interaction', *Proc. Int. Symp. on Pump Noise and Vibrations, Société Hydrotechnique de France (SHF)*, Clamart, 1993, pp. 111–119.
18. T. Yuasa and T. Hinata, 'Fluctuating flow behind the impeller of centrifugal pump', *Bull. JSME*, **22**, 1746–1753 (1974).
19. M. Sideris and R. A. van den Braembussche, 'Influence of a circumferential exit pressure distortion on the flow in an impeller and diffuser', *ASME, J. Eng. Gas Turbines Power*, (1986).
20. R. Dong, S. Chu and J. Katz, 'Quantitative visualization of the flow within the volute of a centrifugal pump. Part A: Technique, Part B: Results and analysis', *J. Fluids Eng.*, **114**, 391–403 (1992).
21. S. M. Miner, R. J. Beaudoin and R. D. Flack, 'Laser velocimeter measurements in a centrifugal flow pump', *J. Turbomach.*, **111**, 205–212 (1989).
22. C. P. Hamkins and R. D. Flack, 'Laser velocimeter measurements in shrouded and unshrouded radial flow pump impellers', *J. Turbomach.*, **109**, 70–76 (1987).